Journal of Thermal Engineering
https://jten.yildiz.edu.tr/
https://doi.org/10.47481/jten.0092

RESEARCH ARTICLE

Analysis of the Magnetohydrodynamics Casson fluid flow with an exponentially accelerated plate incorporating the Soret and Hall effects

Mr. Shital Anant Patil[1,2], Dr. Bharti V. Nathwani[3,*], Dr. Harshad Patel[4]

[1]Department of Mathematics, Amity School of Applied Sciences, Amity University Mumbai, Panvel, Maharashtra 410206, India
[2]Department of Applied Sciences and Humanities, Pimpri Chinchwad College of Engineering and Research, Ravet, Pune, Maharashtra 412101, India
[3]Department of Mathematics, Amity School of Applied Sciences, Amity University Mumbai, Panvel, Maharashtra 410206, India
[4]Department of Mathematics, Shri Govind Guru University, Gujarat 384012, India

Abstract

This article provides study of the Magnetohydrodynamics flow of a Casson fluid influenced by heat and mass transfer in an unsteady free convection environment with a rotating porous medium. The investigation considers different physical parameters like the Soret and Hall phenomena, thermal radiation, and chemical reaction, that are important in biomedical engineering, industrial processing, and magneto-thermal systems. The flow is considered between the exponentially accelerating plates, with both ramped and constant temperature and concentration boundary conditions. A set of coupled dimensionless differential equations that governs the flow are made dimensionless by a similarity transform and then evaluated numerically using MATLAB bvp4bc function. The results prove that the primary velocity enhances with higher hall parameter, permeability, and thermal and solutal Grashof numbers, while the thermal profile declines with enhancing radiation and Prandtl numbers. Also, the concentration levels rise with greater Soret and Schmidt parameters. The novelty of this work is that it combined modelling of reactive, thermodiffusive, and electromagnetic effects in a rotating porous system, which goes beyond earlier research that usually dealt with these phenomena separately.

Keywords: Mass transfer, Grashof number, Prandtl number, Casson fluid, porous medium, Hall parameter, heat generation parameter

Cite this article as: Patil, S. A., Nathwani, B. V., & Patel, H. (2026). Analysis of the magnetohydrodynamics Casson fluid flow with an exponentially accelerated plate incorporating the Soret and Hall effects. Journal of Thermal Engineering, 12(6), 2191–2202. https://doi.org/10.47481/jten.0092

1. Introduction

The study of the Casson fluid models is very important in different fields like biomedical engineering, industrial processes, and environmental systems. A British rheologist, Sidney Gerald Casson, proposed the Casson fluid in 1959 [1] as a non-Newtonian fluid having yield stress. Due to its shear-thinning behavior, it is used in

Application requiring controlled viscosity, such as in blood flow, paints, coatings, and food products. Casson fluids are used in modeling biological flows, especially in capillaries where nutrient transport is influenced by temperature and concentration gradients, and in drug delivery systems.

The non-Newtonian fluids have complex behavior. To describe various properties of these fluids different models are proposed. The Power-law, Herschel–Bulkley, Carreau, and Casson models are few examples. These models help us in understanding flow patterns in food technology, personal care products, and physiological transport systems. Dash et al. [2] examined how a Casson fluid flows across a homogeneous porous material. A non-Darcy porous medium's Casson fluid flow was examined by Makanda et al. [3]. He applied the Brinkman model to see the Darcy resistance caused by a porous medium. Sher Akbar et al. [4] studied the Casson fluid flow in a plumb duct, focusing on physiological transport. Their analysis showed how the Casson fluid parameters affect the velocity and pressure parameter in biomedical applications. The interaction of the

*Corresponding Author
E-mail Adress: bvnathwani@mum.amity.edu

Submitted: 15 May 2025; **Accepted:** 9 September 2025

This paper was recommended for publication in revised form by Editor-in-Chief Ahmet Selim Dalkılıç

Casson fluid flow with magnetohydrodynamics (MHD) increases complexity and its importance. Alfvén [5, 6] coined the term MHD and described the importance of Maxwell's and Navier–Stokes equations in these flows. This concept has applications in space weather prediction, fusion technology, and industrial magneto-fluid systems.

Many researchers have studied MHD fluid dynamics under various physical conditions. Zaheer Abbas et al. [7] investigated the entropy generation in an MHD flow through a vertical porous channel with thermal radiation and slip effects. In their study they showed that radiation and viscous effects increase entropy. The results are proved using mathematical model, but it lacks experimental validation which limits its usefulness. Gireesha et al. [8] used the hermite wavelet approach to analyze entropy formation in the MHD Williamson hybrid nano fluid flow with an inclined channel. It shows the influence of the magnetic field, nanoparticle shape, and other parameters. On nano fluid flow.

Nadeem et al. [9] examined peristaltic MHD flow in an annulus with radially varying magnetic fields, underlines its effect on flow reversal and transport. The model is analytical sound, but it is valid for fluid with low Reynolds number and long wavelength. Nadeem et al. [10] used an analytical method to examine the unstable mixed convection MHD flow across a spinning cone. The study shows the magnetic and rotational effects, but it uses simplified assumptions. Ullah et al. [11] studied how the yield stress, magnetic field, and geometric undulations change the thermal transfer and flow behavior. The work is numerically sound, but it lacks experimental validation and it is limited to specific geometry only. MHD viscoelastic fluid flow across a stretching sheet with varying viscosity was investigated by Prasad et al. [12]. Their findings emphasized significant effects on velocity and temperature, but they have not considered advanced factors such as radiation or chemical reactions. Hayat et al. [13] used thermophoresis to examine how thermal radiation and Joule heating affects the Maxwell fluid flow. The MHD flow of water-based nanofluids including copper and aluminum oxide nanoparticles across a permeable stretching sheet in a porous media was studied by Mathews et al. [14]. Using similarity transformations and MATLAB's bvp4c function,

They display superior thermal performance and velocity profiles compared to base fluid, with findings matching the current literature accurately.

Sandeep et al. [15] examined unsteady magnetic Nanofluid flow over a thin elastic sheet. They showed how the magnetic and elastic effects influence the velocity and temperature profiles using numerical methods. Yadav et al. [16] investigated advanced nanofluid flow with chemical reaction and transport phenomena. This concept has improved the performance of thermal systems across energy, biomedical, and industrial fields. Sandeep et al. [17] investigated the thin-film flow of magnetic nanofluids having graphene nanoparticles under magnetic field. The study proved how the flow and thermal properties are influenced by the magnetic field and nanoparticle concentration. Nagaraju et al. [18] showed that there is negative correlation between magnetic field and fluid velocity due to the Lorentz force, while suction increases the thermal transfer due to thinning of the thermal boundary layer.

Nadeem et al. [19] emphasized the magnetic field, the Casson parameter, and the nanoparticles effect but ignored the thermal radiation effect and unsteady flow. Mohyud-Din [20, 21] considered biaxially stretched sheets with nanoparticle suspensions. Raju [22] devised nonlinear model of fluid flow to include radiation parameter in temperature and concentration equations. Kataria et al. [23] studied nano fluid flow with oscillating vertical plate including radiation and magnetic field parameters. The study effectively analyzes the velocity and thermal profiles but assumes an optically thick medium and simplified boundary conditions. The equations were reduced to ordinary differential equations by Kataria et al. [24] using similarity transformations, and the finite difference technique (FDM) was used to solve them numerically. This study examined how different physical characteristics affected the temperature, velocity, and micro-rotation profile. Kataria et al. [25] examined the MHD Casson fluid flow in porous medium through an oscillating vertical plate, considering the impact of chemical reactions and radiation. They used the Crank–Nicolson FDM for numerical solutions and similarity transformations to make the equations simpler. Heat transmission and entropy formation in hybrid nanofluids were investigated by Gireesha et al. [26]. They examined the effects of the flow characteristics and nanoparticle morphologies on the heat radiation in the inclined flows and stretchable channels using the Taylor and Hermite wavelet methods. In recent times, fractional differential equations (FDEs) have emerged as an effective modeling tool due to their ability to incorporate memory and hereditary properties in real-world systems [27-28]. Among the less explored yet significant phenomena are the Soret and Hall effects. The mass flux caused by thermal gradients is known as the Soret effect (thermal diffusion), and it is essential for multicomponent flows, especially in porous media and nanofluids. It influences the mixing, concentration profiles, and mass transfer rates. The Hall effect, on the other hand, becomes important in regions with low-density or high-magnetic-field, where a transverse electric field changes the current and velocity distribution in the conducting fluids. Several studies have considered these effects. Gireesha et al. [29] investigated entropy generation in tangent-hyperbolic fluid flow through a vertical microchannel under the Hall effect using Taylor wavelet method. Raghunath et al. [30] studied free convection Casson fluid in a magnetic field, showing the thermo-diffusion and Hall currents effect on the velocity and concentration. Siva Reddy et al. [31] used finite element methods to analyze similar effects in MHD flows. Liyaqat Ali et al. [32] explored the micropolar effects on the fluid velocities and thermal profiles. Narayana et al. [33] addressed rotating frames in micropolar flows. Seth et al. [34-35] studied optically thick and rotating fluid flow.

Casson fluids are characterized by yield stress and so the flow is influenced by mass and heat transfer. Heat transfer affects the temperature distribution, while mass transfer affects the concentration gradients. These effects play important role in thermal conductivity and flow control. The concept has applications in blood flow problems, polymer processing, food manufacturing, and bioengineering. This study improves system efficiency, cooling technologies, and design of heat and mass transfer equipment. Bargal et al. [36] proves that the innovative microchannel design with sinusoidal cavities and elliptical ribs using graphene quantum dots nano fluid increases heat transfer and reduces the pressure needed for efficient thermal management. Khalid et al. [37] showed the significance of perfecting the fin geometry and coolant type in heat sinks, proving that semicircular wavy fins with nanofluids enhance the thermal performance. Deka et al. [38] investigation enhances the understanding of MHD flow over inclined surfaces, providing ideas for improving solutal and thermal transmission which has applications in nuclear reactors, chemical processing, and metallurgical engineering systems.

Kataria et al. [39] considered unsteady MHD Casson fluid flow past an oscillating vertical plate in a porous medium. Incorporating radiation and chemical reactions effect. The study shows that the radiation and reaction parameters significantly influence the velocity and the temperature profiles. Hari R. Kataria et al. [40] investigated the Soret and heat generation effect on the unsteady MHD Casson fluid flow. The study found that both parameters significantly affect thermal and solutal profiles. While both the work helps in understanding non-Newtonian MHD flows, it considered ideal conditions, limiting its applications. However, very few studies have analyzed the secondary velocity field under the combined impact of Soret and Hall effects, particularly when the plate oscillates exponentially.

The current article works on the gap found above. It extends the findings of Kataria et al. [39-40] by considering the influence of the Hall current, Casson parameter, magnetic parameter, permeability, and rotation on the velocity, temperature, and concentration profiles of the Casson fluid. The fluid flows past a vertically oscillating plate with ramped temperature and concentration boundary conditions. The finite element method (FEM) (with the help of pdepe function in MATLAB) is used to solve the governing partial differential equations numerically after they have been converted using the proper similarity transformations. The results are thoroughly debated and verified against data that has already been published. The novelty of this article is that this study represents the first comprehensive investigation combining exponentially accelerating plate dynamics with secondary velocity field analysis, simultaneous incorporation of Soret and Hall effects in MHD Casson fluid flow, Coupled thermodiffusive and electromagnetic effects in the rotating porous media and both ramped and constant boundary conditions for the temperature and concentration. Our literature review confirms that no earlier study has simultaneously addressed all these phenomena in a single comprehensive model. While individual effects have been studied in isolation, the synergistic interaction of exponentially accelerating plates with combined Soret-Hall effects in the Casson fluid is a significant gap that our work addresses.

The sections of this article are arranged as follows: The Introduction section provides the background and motivation for this study; the Problem Statement section describes the physical setup and mathematical modeling of the problem; the Solution Methodology provides how the mathematical modeling is solved using numerical methods; the Results and Discussion section interprets the physical behavior through graphical analysis; and the Conclusion summarizes the key findings.

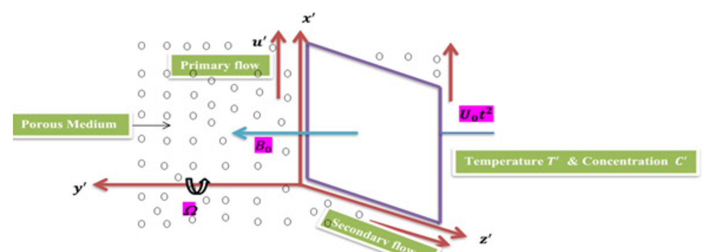

Figure 1. The pictorial representation of the experiment

2. Problem statement

The z' axis stands perpendicular to the x'y' plane, with a plate aligned along the x' axis. A fluid rotates about the y' axis in conjunction with the plate. The figure provides a visual depiction of this experimental setup. When the experiment starts, i. e., at $t' \leq 0$ both the primary and secondary velocities are zero, temperature T'_∞, and concentration is C'_∞. Along the boundary $y' = 0$, the fluid is exponentially accelerated, the secondary velocity is zero, the temperature and concentration are the ramped temperature and the ramped concentration respectively. Another boundary condition is at infinity, i.e. $y' \to \infty$, primary and secondary velocities tend to zero, the temperature tends to T'_∞ and concentration tends to. The Casson fluid model is

$$\tau_{ij} = \begin{cases} 2\left(\mu_c + \dfrac{p_y}{\sqrt{2\pi}}\right)e_{ij}, & \pi > \pi_c \\ 2\left(\mu_c + \dfrac{p_y}{\sqrt{2\pi_c}}\right)e_{ij}, & \pi < \pi_c \end{cases}$$

where p_y, μ_c, e_{ij} is yield stress, viscosity of Casson fluid and elements of the rate of deformation respectively.

$$\rho\frac{\partial u'}{\partial t'} + 2\Omega v' = \mu_B\left(1 + \frac{1}{\gamma}\right)\frac{\partial^2 u'}{\partial y'^2} - \frac{\sigma B_0^2}{(1+m^2)}(u' + mv') - \frac{\mu_B}{k'_1}u' + g\rho\beta'_T(T' - T'_\infty) + g\rho\beta'_C(C' - C'_\infty) \quad (1)$$

The fluid's equations of motion are as follows:

$$\rho\frac{\partial v'}{\partial t'} - 2\Omega u' = \mu_B\left(1 + \frac{1}{\gamma}\right)\frac{\partial^2 v'}{\partial y'^2} + \frac{\sigma B_0^2}{(1+m^2)}(mu' - v') - \frac{\mu_B}{k'_1}v' \quad (2)$$

$$\frac{\partial T'}{\partial t'} = \frac{k}{\rho C_p}\frac{\partial^2 T'}{\partial y'^2} - \frac{1}{\rho C_p}\frac{\partial q_r}{\partial y'} + \frac{Q_0}{\rho C_p}(T' - T'_\infty) \quad (3)$$

$$\frac{\partial C'}{\partial t'} = D_M\frac{\partial^2 C'}{\partial y'^2} + D_T\frac{\partial^2 T'}{\partial y'^2} - k'_2(C' - C'_\infty) \quad (4)$$

The initial conditions are

$$u' = 0,\ v' = 0,\ T' = T'_\infty,\ C' = C'_\infty;\ \text{as } y' \geq 0 \text{ and } t' \leq 0$$

The boundary condition at one end $y' = 0$ and for $t' \leq 0$ is

$$u' = U_0 e^{at'}, \qquad v' = 0,$$

$$T' = \begin{cases} T'_\infty + (T'_w - T'_\infty)\dfrac{t'}{t_0}, & 0 < t' < t_0 \\ T'_w, & t' \geq t_0 \end{cases}$$

$$C' = \begin{cases} C'_\infty + (C'_w - C'_\infty)\dfrac{t'}{t_0}, & 0 < t' < t_0 \\ C'_w, & t' \geq t_0 \end{cases} \quad (6)$$

Another Boundary Condition at other end $y' \to \infty$ and $t' \geq 0$ is

$$u' \to 0,\ v' \to 0,\ T' \to T'_\infty,\ C' \to C'_\infty \quad (7)$$

Dimensionless similarity transformations simplify the partial differential equations by reducing the variables. This process reveals key dimensionless numbers, highlighting the dominant physical effects, improving the calculation efficiency, and enabling the generalization of the results across distinct systems. Using dimensionless quantities as

$$y = \frac{y'}{U_0 t_0},\ t = \frac{t'}{t_0},\ u = \frac{u'}{U_0},\ v = \frac{v'}{U_0},$$

$$\theta = \frac{T' - T'_\infty}{T'_w - T'_\infty},\ C = \frac{C' - C'_\infty}{C'_w - C'_\infty}$$

It reduces the PDEs into

$$\frac{\partial u}{\partial t} + 2k^2 v = \left(1 + \frac{1}{\gamma}\right)\frac{\partial^2 u}{\partial y^2} - \frac{M^2}{(1+m^2)}(u + mv) - \frac{1}{k_1}u + G_r\theta + G_m C \quad (8)$$

$$\frac{\partial v}{\partial t} - 2k^2 u = \left(1 + \frac{1}{\gamma}\right)\frac{\partial^2 v}{\partial y^2} + \frac{M^2}{(1+m^2)}(mu - v) - \frac{1}{k_1}v \quad (9)$$

$$\frac{\partial \theta}{\partial t} = \frac{1}{P_r}\frac{\partial^2 \theta}{\partial y^2} + \left(\frac{H - R}{P_r}\right)\theta \quad (10)$$

$$\frac{\partial C}{\partial t} = \frac{1}{S_c}\frac{\partial^2 C}{\partial y^2} + S_r\frac{\partial^2 \theta}{\partial y^2} - k_r C \quad (11)$$

With the dimensionless first condition for $y \geq 0$ and $t \leq 0$ is

$$u = 0, \quad v = 0, \quad \theta = 0,\ C = 0 \quad (12)$$

The dimensionless boundary conditions for is

$$u = e^{at}, \qquad v = 0,$$

$$\theta = \begin{cases} t, & 0 < t < 1 \\ 1, & t \geq 1 \end{cases} = tH(t) - (t-1)H(t-1),$$

$$\theta = \begin{cases} t, & 0 < t < 1 \\ 1, & t \geq 1 \end{cases} = tH(t) - (t-1)H(t-1),$$

where H(t) is Heaviside function.

Another dimensionless boundary conditions for $y \to \infty$ and $t \geq 0$ is

The parameters used above are

$$u \to 0, \qquad v \to 0, \qquad \theta \to 0, \qquad C \to 0 \quad (14)$$

$$G_r = \frac{\vartheta g\beta'_T(T'_w - T'_\infty)}{U_0^3},\ G_m = \frac{\vartheta g\beta'_C(C'_w - C'_\infty)}{U_0^3},$$

$$G_r = \frac{\vartheta g\beta'_T(T'_w - T'_\infty)}{U_0^3},\ G_m = \frac{\vartheta g\beta'_C(C'_w - C'_\infty)}{U_0^3}, P_r = \frac{\rho\vartheta C_p}{k},\ H = \frac{Q_0\vartheta^2}{kU_0^2},\ S_c = \frac{\vartheta}{D_M},\ K_r = \frac{\vartheta k'_2}{U_0^2},$$

$$\alpha = \frac{\alpha_1}{\rho},\ k_1 = \frac{\vartheta\phi}{k'_1},\ \vartheta = U_0^2 t_0,$$

$$k^2 = \frac{\Omega t_0}{\rho},\ \mu_B = \rho\vartheta,\ k_1 = \frac{k'_1\rho U_0^2}{\mu_B\vartheta} \quad (15)$$

3. Solution of the problem

When Casson fluid flow problem is modeled in mathematical form, it boils down to a set of partial differential equations (PDE). They are reduced into the linear dimensionless set of PDE (8) to (11) with the initial and boundary conditions (12) to (14). The equations can be solved analytically or numerically. Obtaining an analytic solution in most cases is difficult. Even if we obtain an analytic solution, interpreting the results is also a cumbersome task. The Laplace transform can be applied to get analytic solutions. However, it is difficult to draw graphs form an analytic solution for various values of the parameters, while with numerical methods (and with the help of MATLAB) it is comparatively easy to draw graphs and interpret the results.

3.1. Solution of the MHD flow problem with the Ramped Temperature and Ramped Concentration

As we have seen previously, the dimensionless similarity transformation reduces the set of PDE to a dimensionless form. MATLAB software is used to solve these dimensionless equations using the finite element method. The pdepe function is a powerful tool in MATLAB used for numerically solving partial differential equations in one spatial dimension and time. It is particularly valuable for modeling parabolic and elliptic PDEs, which commonly arise in heat transfer, mass diffusion, and fluid flow problems. By handling the spatial and temporal discretization automatically, pdepe simplifies the solution of complex, coupled PDE systems. Its built-in numerical solvers ensure accuracy and stability, making it highly useful in engineering, physics, and applied mathematics. While using the pdepe function, an increment size of 0.111 is taken for the temporal variable t and an increment size of 0.0159 is taken for the spatial variable y. Here, the cost and accuracy of the solution are heavily influenced by the length of y.

3.2. Solution of the MHD flow problem with constant temperature and constant concentration

To understand the effects of ramped temperature and ramped concentration, the findings must be compared with constant temperature and constant concentration. The first and boundary conditions in this case are as follows: the dimensionless first condition for $y \geq 0$ and $t \leq 0$ is

$$u = 0, \quad v = 0, \quad \theta = 0, \quad C = 0 \tag{16}$$

The dimensionless boundary conditions for

$y = 0$ and $t \geq 0$ is

$$u = e^{at}, \quad v = 0, \quad \theta = 1, \quad C = 1 \tag{17}$$

Another boundary condition for $y \to \infty$ and $t \geq 0$ is

$$u \to 0, \quad v \to 0, \quad \theta \to 0, \quad C \to 0 \tag{18}$$

The set of dimensionless PDE is solved using the same discretization that we have already used for the ramped case.

4. Numerical results and discussion

For both ramping and constant temperature and concentration settings, a graphic representation is provided of how the Soret and Hall currents affect the velocity, temperature profile, and concentration profile. A parametric study is carried out to gain a comprehensive understanding of the physics involved in the situation, and graphical explanations of the numerical results are given. Figures 2–19 display the primary velocity, secondary velocity, fluid temperature, and concentration using various parameters.

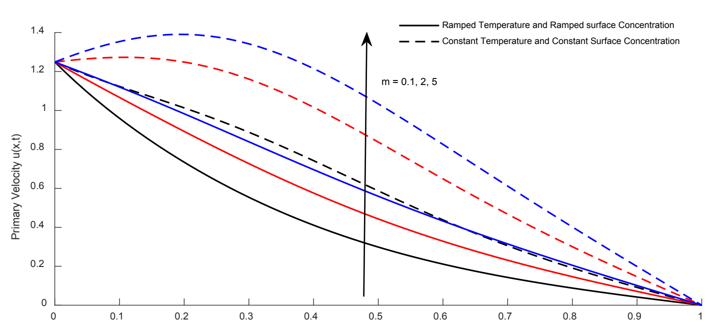

Figure 2. Graph of Primary velocity Vs the Hall parameter m

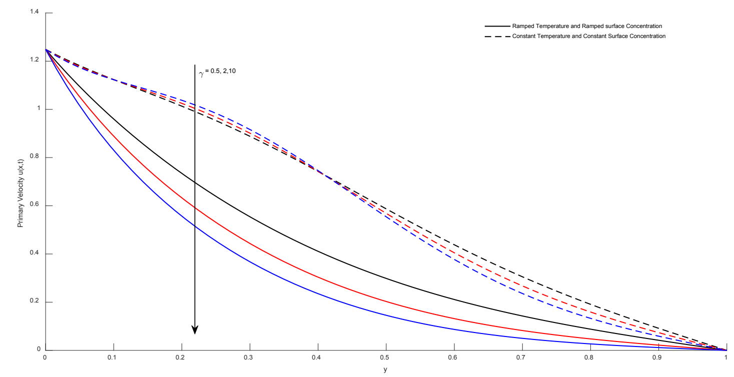

Figure 3. Graph of Primary velocity Vs the Casson fluid parameter γ

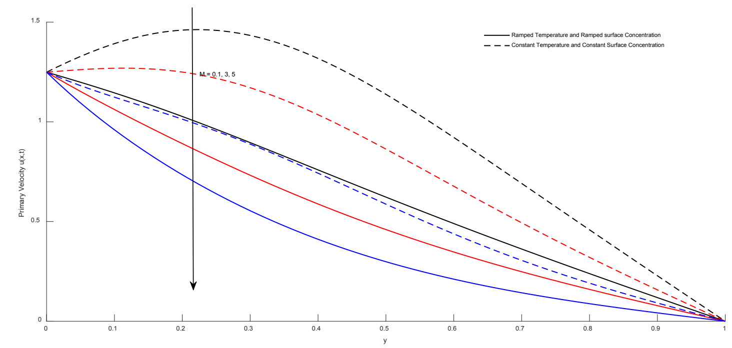

Figure 4. Graph of Primary velocity Vs the Magnetic fluid parameter M

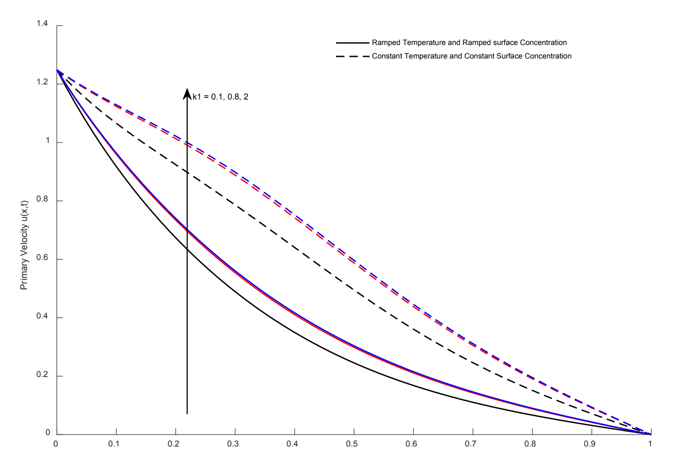

Figure 5. Graph of Primary velocity Vs the permeability parameter k1

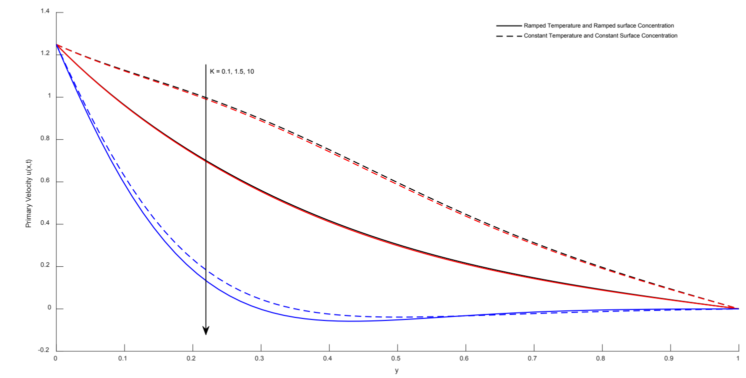

Figure 6. Graph of Primary velocity Vs the rotation parameter k

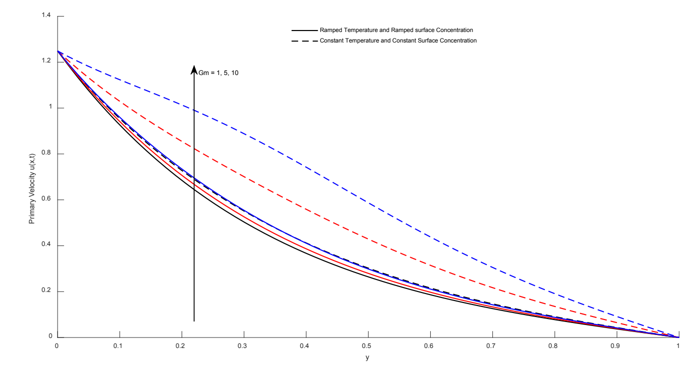

Figure 7. Graph of Primary velocity Vs the heat transfer Grashof number Gr

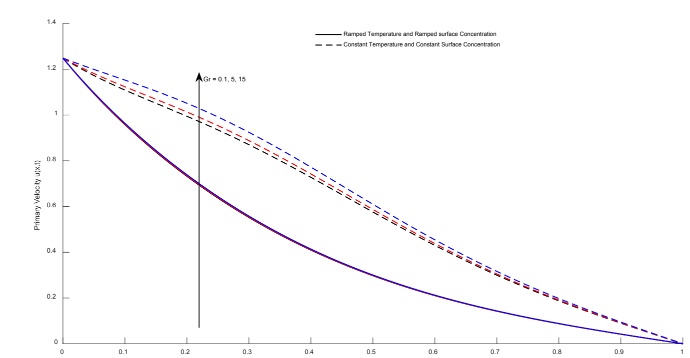

Figure 8. Graph of Primary velocity Vs the mass transfer Grashof number Gm

Figures 2 through 19 illustrate that fluids kept at a constant temperature show higher rates of mass transfer, heat transfer, and momentum compared to MHD fluids with ramped boundary conditions. For the concentration profiles, a similar pattern is noted. The reason being, for constant temperature and concentration, the system achieves a steady-state MHD flow, resulting in a stable velocity profile. The momentum transfer increases due to stability. Similarly, a uniform temperature distribution increases the heat transfer, and a uniform concentration gradient enhances mass transfer. Whereas the non-uniform flow in ramped temperature and concentration reduces the overall momentum and transport profile.

Figure 2 shows the relation between the Hall current parameter m and the primary velocity u(x,t), when all other parameters are constant. It is found that an increase in m results in an enhanced velocity profile. A stronger Hall current reduces the resistive forces in the fluid, which allows the magnetic field to induce more electric currents. These currents generate a Lorentz force that enhances the fluid motion. This has practical applications in areas such as MHD propulsion systems, plasma physics, electromagnetic flow control, and plasma-based manufacturing.

In Figure 3, the Casson parameter γ decreases as the primary velocity increases. As γ increases, the fluid's yield stress enhances, which opposes motion of the fluid. The Casson fluid's velocity is reduced due to this added resistance. This has applications in designing systems involving non-Newtonian fluids, such as in biomedical or food engineering.

Figure 4 shows the correlation between the magnetic parameter M and the primary velocity u(x, t). As M increases, the fluid motion is opposed by the increased magnetic drag force, so the velocity and the boundary layer thickness decline. This concept has applications in electromagnetic braking systems in high-speed trains, MHD power generation, nuclear reactor cooling systems, and electrochemical processes such as electroplating.

Figure 5 shows the direct relationship between the permeability parameter k1 and primary velocity. As the permeability parameter enhances, the porous medium's resistance lowers, thus it develops momentum boundary layer. This increased fluid velocity and a thicker boundary layer is important for oil recovery, filtering systems, and flow in porous biological tissues.

There is inverse correlation between rotation parameter k and primary velocity which is clear from Figure 6. As k decreases, the fluid experiences reduce rotational effects, declining the viscosity and enhancing the velocity.

The effect of the thermal Grashof number, which is the ratio of buoyancy to the viscous forces developed due to the temperature gradients, is covered in Figure 7. A higher Grashof number shows that the buoyant force is dominant, which enhances fluid acceleration. This has applications in the cooling of electronic components, solar energy harvesting, chimney design, and geothermal systems.

Figure 8 illustrates the relation between the mass transfer Grashof number and velocity profile. Here also the higher Grashof number shows greater buoyant forces in relation to viscous resistance, which increases fluid velocity. This concept is important in atmospheric pollutant dispersion, chemical absorption processes, and thermal management in food packaging and preservation systems.

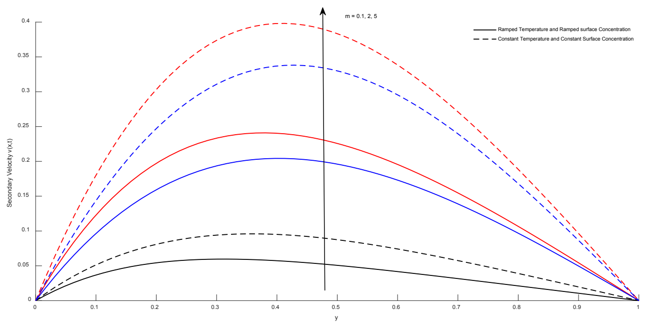

Figure 9. Graph of Secondary velocity v(x,t) Vs the Hall current parameter m

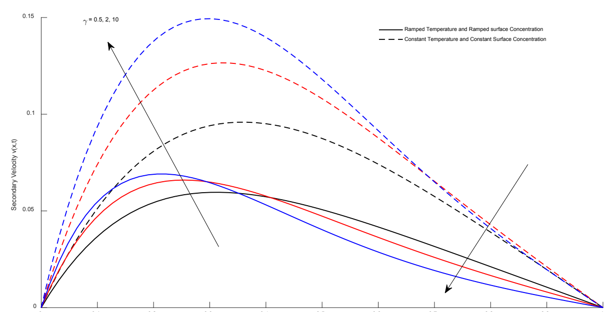

Figure 10. Graph of Secondary velocity v(x,t) Vs the Casson fluid parameter

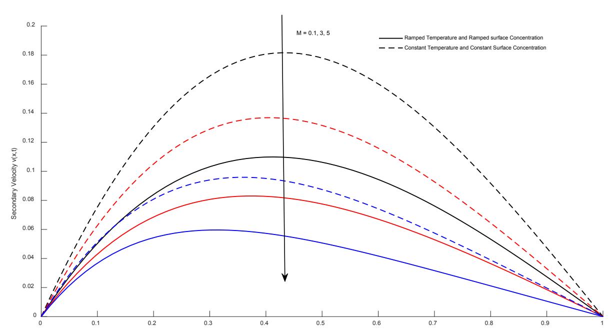

Figure 11. Graph of Secondary velocity v(x,t) Vs the magnetic fluid parameter M

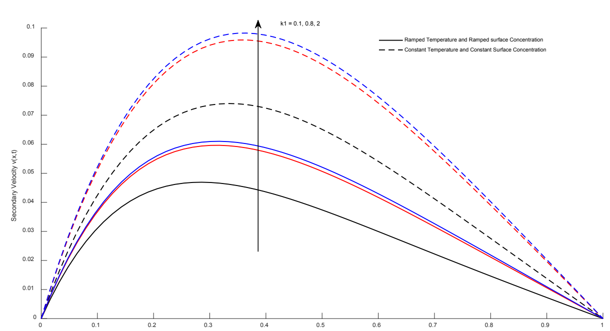

Figure 12. Graph of Secondary velocity v(x,t) Vs the permeability parameter k1

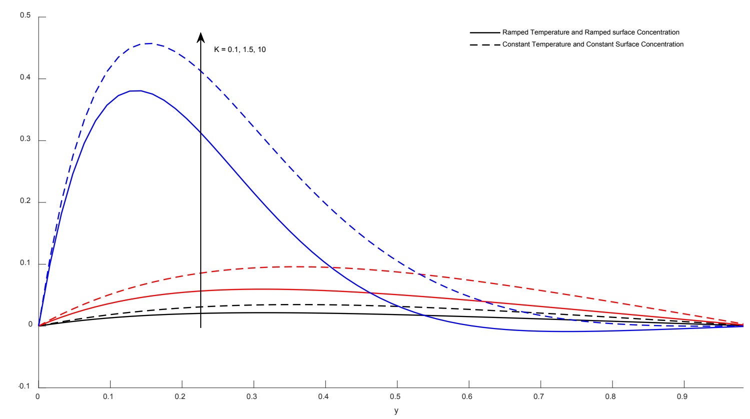

Figure 13. Graph of Secondary velocity v(x,t) Vs the rotation parameter k

When all other parameters are held constant, Figure 9 shows correlation between secondary velocity v(x,t) and the Hall current parameter m. Both have positive correlations. This is because the enhanced Hall effect reduces the fluid's electromagnetic resistance, which results in a stronger Lorentz force which enhances both the primary and secondary velocity.

Figure 10 presents correlation between the secondary velocity v(x,t) and the Casson fluid parameter γ. In the region, there is a positive correlation—the secondary velocity enhances with the Casson parameter γ. However, beyond, the trend reverses, and the secondary velocity begins to decline. This shows that the yield stress becomes more dominant at far distance from plate, which reduces velocity.

In Figure 11, it is seen that there is negative correlation between the secondary velocity and the magnetic parameter M. The reduction in velocity can be explained by the enhancing magnetic damping force, which reduces the fluid velocity in both the primary and secondary directions due to the higher Lorentz drag.

The association between the permeability parameter k1 and secondary velocity is clear from Figure 12. As rises, the resistance of the porous medium decreases, which enhances momentum diffusion and results in a higher secondary velocity. This result is same as saw in case of primary velocity also.

The association between the rotation parameter k and the secondary velocity is seen in Figure 13. There is a positive link between the secondary velocity and the rotation parameter values. This is because the rotational effects give the fluid more angular momentum, which increases the system's transverse motion (secondary flow).

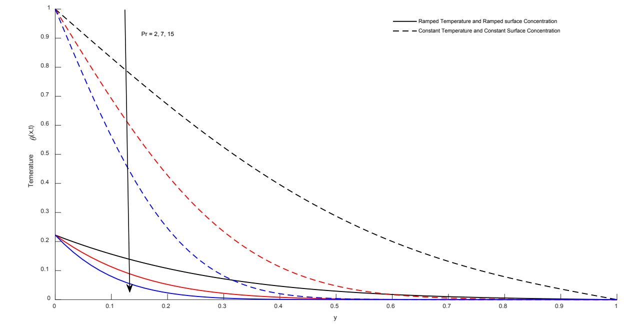

Figure 14. Graph of the temperature profile Vs the Prandtl number Pr

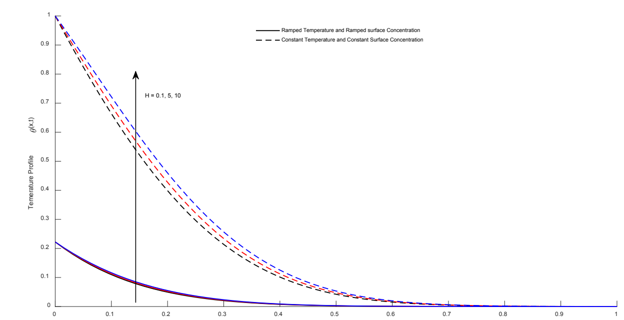

Figure 15. Graph of the temperature profile Vs the heat generation parameter H

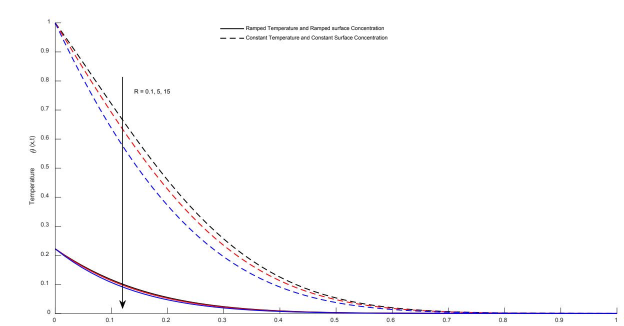

Figure 16. Graph of the temperature profile Vs the radiation parameter R.

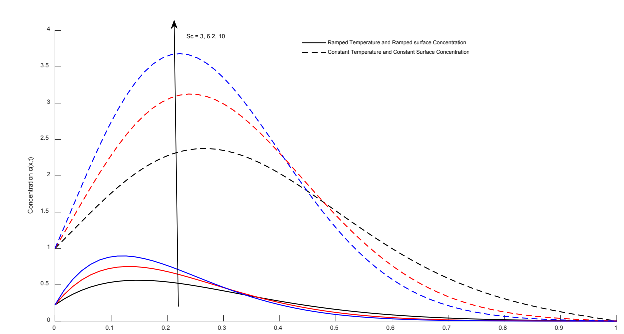

Figure 17. Graph of the concentration profile C(x,t) Vs the Schmidt parameter Sc

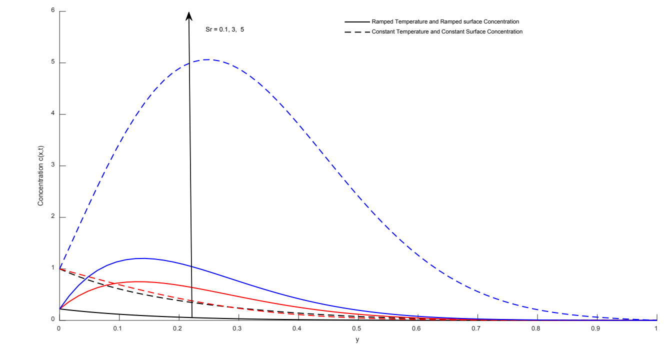

Figure 18. Graph of the concentration profile C(x,t) Vs the Soret parameter Sr

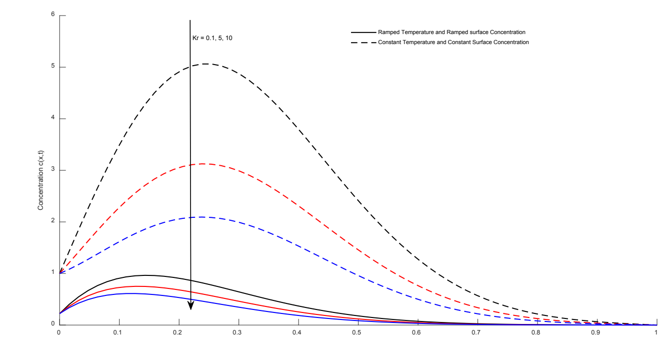

Figure 19. Graph of the concentration profile C(x,t) Vs the chemical reaction parameter Kr

The Prandtl number is the ratio of momentum diffusivity to thermal diffusivity in a fluid. A negative correlation between the temperature profile and the Prandtl number Pr is clear in Figure 14. This happens because heat spreads more slowly in fluids with higher Prandtl numbers. As a result, the thermal boundary layer becomes thinner, and the overall temperature distribution reduces. This concept has applications in coolant design for nuclear reactors, heat exchangers, geophysical flows, semiconductor crystal production, and liquid metal cooling in nuclear fusion systems.

The heat generation parameter H is measure of internal heat generation due to chemical reactions, resistive heating, or nuclear processes. Figure 15 proves a positive correlation. As H increases, it raises internal energy and the temperature of the fluid. This phenomenon has applications in internal combustion engines, battery systems in electric vehicles, electronics cooling (such as microprocessors), and nuclear reactor thermal management.

Figure 16 shows that there is negative correlation between the radiation heat parameter and the temperature profile. As radiation increases, the fluid loses more heat, leading to a drop in temperature. This concept has applications in regulating the temperature in industrial furnaces, preventing thermal damage to spacecraft during atmospheric re-entry, and managing excess heat in solar panels.

The Schmidt number is the ratio of momentum diffusivity to the mass diffusivity. It is important in the mass transfer analysis. Figure 17 shows that as Sc enhances, the concentration profile steepens, showing slower mass diffusion. Higher Schmidt numbers show that momentum diffusion is more as compared to mass diffusion. The concept has applications in separation processes, fuel mixing in combustion, and pollutant dispersion modeling.

The Soret effect, or thermophoresis, shows movement of particles due to a temperature gradient. The Soret parameter (Sr) quantifies the effect of temperature gradient on mass transfer in a fluid. Figure 18 depicts that as Sr enhances; the concentration profile is also improved. This will enhance mass transfer due to temperature gradients. This concept has applications in nanofluid technology, multicomponent fluid flows, and biological systems.

Finally, Figure 19 examines the influence of the chemical reaction parameter kr on concentration profile. Chemical reaction parameter is the ratio of the rate of chemical reaction to rate of mass diffusion. A positive correlation was seen between kr and the rate of concentration profile. As kr increases, the reactants are consumed more rapidly, which decreases the concentration of the species. This has applications in perfecting catalytic processes, environmental remediation, and pharmaceutical manufacturing.

5. Conclusion

This study investigates the unsteady MHD Casson fluid flow over a quadratically accelerating vertical plate including physical parameters like thermal radiation, magnetic field, and chemical reactions, with ramped temperature and concentration conditions. It is found that, the primary velocity increases with the Hall current parameter, permeability parameter, and Grashof numbers for heat and mass transfer. This concept has applications in electromagnetic pumps, cooling systems, porous media filtration, rotating machinery, and non-Newtonian fluid control in engineering processes. The primary velocity decreases with the Casson parameter, magnetic fluid, and rotation parameters. The secondary velocity increases with the Hall parameter, permeability and the rotation parameter, due to Coriolis forces. Lower magnetic parameter reduces the opposing force, which increases secondary velocity. This concept has applications in MHD propulsion, plasma control, rotating machinery cooling, polymer processing, and biomedical flows. The temperature profile increases with the heat generation parameter, showing enhanced internal energy. while it decreases with higher Prandtl and radiation parameters due to reduced thermal diffusivity. Concentration profile improves with higher Schmidt and Soret numbers but decline with increased chemical reaction parameters. Ramped boundary conditions slow momentum, heat, and mass transfer, which is relevant in systems requiring gradual thermal or concentration gradients. In future, there is scope to study Casson fluid flow with Soret, Dufor, thermal radiation effects and with various boundary conditions like Quadratically accelerated plate, multislip conditions. In addition to this, Fractional differential equations (FDEs) can be employed to study memory-dependent behavior of Casson fluid flow.

Authorship contributions

Author-wise contribution is as follows

Shital Anant Patil: Conceptualization; Methodology; Discussion of Results; Writing Original Draft; Writing Review and Editing; Approval of the Final Text. Bharti V. Nathwani: Methodology; Writing Review and Editing; Supervision; Approval of the Final Text. Harshad Patel: Conceptualization; Discussion of Results; Writing Original Draft; Supervision; Approval of the Final Text.

Data availability statement

The data supporting the findings of this study are available from the corresponding author upon reasonable request.

Conflict of interest

The author declared no potential conflicts of interest with respect to the research, authorship, and/or publication of this article.

Acknowledgement

The authors declare that this research was conducted independently and did not receive any form of aid, support, or funding from any individual, institution, or organization. All work presented in this paper is solely the result of the authors' own efforts.

Use of AI models

The authors used ChatGPT only for language editing and improving the readability of the manuscript. All scientific content, data analysis, interpretation, and conclusions were developed and verified by the authors, who take full responsibility for the manuscript.

Nomenclature

u'	Primary velocity (m/s)
v'	Secondary velocity (m/s)
t'	Time (seconds)
T'	Temperature (k kelvin)
C'	Concentration (kg/
μ_B	Dynamic Viscosity (kg/ms)
γ	Casson Fluid Parameter (Pa)
σ	Electrical Conductivity (S/m)
B_0	Uniform Magnetic Field (T Tesla)
g	Force Due to gravity (
ρ	Density of Fluid (kg/m^3)
β'_T	Thermal expansion coefficient (1/K)
β'_C	Concentration expansion coefficient (m^3/kg)
C_p	Isobaric specific heat (J/kgK)
q_r	Radiative Heat Flux (W/m^2)
D_M	Coefficient of Mass Diffusivity (m^2/s)
D_T	Coefficient of Thermal Diffusivity (m^2/s)
ϑ	Kinematic Viscosity (m^2/s)
k	Permeability of the Porous Medium Parameter (m^2)
u	Dimensionless primary velocity
v	Dimensionless secondary velocity
t	Dimensionless Time
θ	Dimensionless Temperature
C	Dimensionless Concentration
m	Hall Current Parameter
M	Magnetic parameter
G_m	Mass Transfer Grashof number
G_r	Heat Transfer Grashof number
P_r	Prandtl Number
H	Heat generation parameter
R	Radiation Parameter
S_C	Schmidt number
S_r	Soret Parameter
k_r	Chemical reaction parameter

References

[1] Casson, N. (1959), A Flow Equation for Pigment-Oil Suspensions of the Printing Ink Type. In: Mill, C.C., Ed., Rheology of Disperse Systems, Pergamon Press, Oxford, 84-104.

[2] Dash, K.N. Mehta, G. Jayaraman, Casson fluid flow in a pipe filled with a homogeneous porous medium, International Journal of Engineering Science, Volume 34, Issue 10, 1996, Pages 1145-156, ISSN 0020-7225, https://doi.org/10.1016/0020-7225(96)00012-2.R.

[3] Makanda, Gilbert, Shaw, Sachin, Sibanda, Precious, Diffusion of Chemically Reactive Species in Casson Fluid Flow over an Unsteady Stretching Surface in Porous Medium in the Presence of a Magnetic Field, Mathematical Problems in Engineering, 2015, 724596,10 pages, 2015. https://doi.org/10.1155/2015/724596

[4] Sher Akbar, N. and Adil Wahid, B., Physiological Transportation of Casson Fluid in a Plumb Duct, Communications in Theoretical Physics, vol. 63, no. 3, Art. no. 347, IOP, 2015. doi:10.1088/0253-6102/63/3/347

[5] ALFVÉN, H. Existence of Electromagnetic-Hydrodynamic Waves. Nature 150, 405–406 (1942). https://doi.org/10.1038/150405d0

[6] Alfvén, Hannes (1943). "On the Existence of Electromagnetic-Hydrodynamic waves" (PDF). Arkiv för matematik, astronomi och fysik. 29B (2): 1–7.

[7] Zaheer Abbas, Muhammad Naveed, Meriyem Hussain, Nadeem Salamat, Analysis of Entropy generation for MHD flow of viscous fluid embedded in a vertical porous channel with thermal radiation, Alexandria Engineering Journal, Volume 59, Issue 5, 2020, Pages 3395-3405, ISSN 1110-0168, https://doi.org/10.1016/j.aej.2020.05.019.

[8] Lakshmi, R., Gireesha, B.J., Venkatesh, P. et al. Hermite Wavelet Approach to Analyze the Entropy Generation of MHD Williamson Hybrid Nanofluid Flow through an Inclined Channel with Particle Shape Effects. Int. J. Appl. Comput. Math 11, 40 (2025). https://doi.org/10.1007/s40819-025-01853-6

[9] Nadeem, Noreen Sher Akbar, Influence of radially varying MHD on the peristaltic flow in an annulus with heat and mass transfer, Journal of the Taiwan Institute of Chemical Engineers, Volume 41, Issue 3, 2010, Pages 286-294, ISSN 1876-1070, https://doi.org/10.1016/j.jtice.2009.11.004.S.

[10] Nadeem, S. Saleem, Analytical treatment of unsteady mixed convection MHD flow on a rotating cone in a rotating frame, Journal of the Taiwan Institute of Chemical Engineers, Volume 44, Issue 4, 2013, Pages 596-604, ISSN 1876-1070, https://doi.org/10.1016/j.jtice.2013.01.007.

[11] Inayat Ullah, M. Arif, Sohail Nadeem, Jehad Alzabut, Numerical computations of MHD mixed convection flow of Bingham fluid in a porous square chamber with a wavy cylinder, International Journal of Thermofluids, Volume 24, 2024, 100938, ISSN 2666-2027, https://doi.org/10.1016/j.ijft.2024.100938.

[12] Prasad, Dulal Pal, V. Umesh, N.S. Prasanna Rao, The effect of variable viscosity on MHD viscoelastic fluid flow and heat transfer over a stretching sheet, Communications in Nonlinear Science and Numerical Simulation, Volume 15, Issue 2, 2010, Pages 331-344, ISSN 1007-5704, https://doi.org/10.1016/j.cnsns.2009.04.003

[13] Hayat, M. Qasim, Influence of thermal radiation and Joule heating on MHD flow of a Maxwell fluid in the presence of thermophoresis, International Journal of Heat and Mass Transfer, Volume 53, Issues 21–22, 2010, Pages 4780-4788, ISSN 0017-9310, https://doi.org/10.1016/j.ijheatmasstransfer.2010.06.014.

[14] Mathews J, Talla H. Unsteady magnetohydrodynamic free convection flow of Al2O3–Cu/water nanofluid over a permeable linear stretching sheet through a porous medium with viscous dissipation and heat source/sink. J Ther Eng 2025;11(2):344–356.

[15] Sandeep, I.L. Animasaun, M.E. Ali (2017). Unsteady Liquid Film Flow of Electrically Conducting Magnetic-Nanofluids in the Vicinity of a Thin Elastic Sheet. Journal of Computational and Theoretical Nanoscience. 14. 1140 - 1147. 10.1166/jctn.2017.6418.

[16] Yadav S, Kumar S, Sharma PK, Makkar V, Dang K. Numerical modelling of 3D magnetohydrodynamics chemically reacting permeable sheet influenced by free stream convection nanofluid flow. J Ther Eng 2025;11(3):845–857

[17] Sandeep, Effect of aligned magnetic field on liquid thin film flow of magnetic nanofluids embedded with graphene nanoparticles, Advanced Powder Technology, Volume 28, Issue 3, 2017, Pages 865-875, ISSN 0921-8831, ttps://doi.org/10.1016/j.apt.2016.12.012.

[18] Nagaraju, Mahesh Garvandha, Magnetohydrodynamic viscous fluid flow and heat transfer in a circular pipe under an externally applied constant suction, Heliyon, Volume 5, Issue 2, 2019, e01281, ISSN 2405-8440, https://doi.org/10.1016/j.heliyon.2019.e01281.
[19] Nadeem, S. (2014) MHD Three-Dimensional Boundary Layer Flow of Casson Nanofluid Past a Linearly Stretching Sheet with Convective Boundary Condition. IEEE Transactions on Nanotechnology, 13, 109-115., http://dx.doi.org/10.1109/TNANO.2013.2293735
[20] Syed Tauseef Mohyud-Din, Sheikh Irfanullah Khan, Nonlinear radiation effects on squeezing flow of a Casson fluid between parallel disks, Aerospace Science and Technology, Volume 48, 2016, Pages 186-192, ISSN 1270-9638, https://doi.org/10.1016/j.ast.2015.10.019.
[21] Naveed Ahmed, Umar Khan, Sheikh Irfanullah Khan, Saima Bano, Syed Tauseef Mohyud-Din, Effects on magnetic field in squeezing flow of a Casson fluid between parallel plates, Journal of King Saud University - Science, Volume 29, Issue 1, 2017, Pages 119-125, ISSN 1018-3647, https://doi.org/10.1016/j.jksus.2015.03.006.
[22] C.S.K. Raju, N. Sandeep, S. Saleem, Effects of induced magnetic field and homogeneous–heterogeneous reactions on stagnation flow of a Casson fluid, Engineering Science and Technology, an International Journal, Volume 19, Issue 2, 2016, Pages 875-887, ISSN 2215-0986, https://doi.org/10.1016/j.jestch.2015.12.004.
[23] Hari R. Kataria, Akhil S. Mittal, Mathematical model for velocity and temperature of gravity-driven convective optically thick nanofluid flow past an oscillating vertical plate in presence of magnetic field and radiation, Journal of the Nigerian Mathematical Society, Volume 34, Issue 3, 2015, Pages 303-317, ISSN 0189-8965, https://doi.org/10.1016/j.jnnms.2015.08.005.
[24] Hari R. Kataria, Harshad R. Patel, Rajiv Singh, Effect of magnetic field on unsteady natural convective flow of a micropolar fluid between two vertical walls, Ain Shams Engineering Journal, Volume 8, Issue 1, 2017, Pages 87-102, ISSN 2090-4479, https://doi.org/10.1016/j.asej.2015.08.013.
[25] Hari R. Kataria, Harshad R. Patel, Radiation and chemical reaction effects on MHD Casson fluid flow past an oscillating vertical plate embedded in porous medium, Alexandria Engineering Journal, Volume 55, Issue 1, 2016, Pages 583-595, ISSN 1110-0168, https://doi.org/10.1016/j.aej.2016.01.019.
[26] Gireesha, B. & Kalkere Jayanna, Gowtham. (2025). Thermal radiation impact on hybrid nanocomposite flow in stretchable channels: a Darcy-Forchheimer model with the Taylor wavelet approach. Applied Mathematics and Mechanics. 46. 1107-1124. 10.1007/s10483-025-3260-7.
[27] Samuel Chávez-Vázquez, Jorge E. Lavín-Delgado, José F. Gómez-Aguilar, José R. Razo-Hernández, Sina Etemad, Shahram Rezapour, Trajectory tracking of Stanford robot manipulator by fractional-order sliding mode control, Applied Mathematical Modelling, Volume 120, 2023, Pages 436-462, ISSN 0307-904X, https://doi.org/10.1016/j.apm.2023.04.001.
[28] Hasib Khan, Khurshaid Alam, Haseena Gulzar, Sina Etemad, Shahram Rezapour, A case study of fractal-fractional tuberculosis model in China: Existence and stability theories along with numerical simulations, Mathematics and Computers in Simulation, Volume 198, 2022, Pages 455-473, ISSN 0378-4754, https://doi.org/10.1016/j.matcom.2022.03.009.
[29] Gireesha, B. J., & Gowtham, K. J. (2025). Entropy generation analysis of hyperbolic tangent fluid in upright microchannel with Hall effect by Taylor wavelet collocation method. International Journal of Ambient Energy, 46(1). https://doi.org/10.1080/01430750.2025.2495825.
[30] Kodi Raghunath, Ravuri Mohanaramana, Hall, Soret, and rotational effects on unsteady MHD rotating flow of a second-grade fluid through a porous medium in the presence of chemical reaction and aligned magnetic field, International Communications in Heat and Mass Transfer, Volume 137, 2022, 106287, ISSN 0735-1933, https://doi.org/10.1016/j.icheatmasstransfer.2022.106287.
[31] Siva Reddy Sheri, Megaraju P, Rajashekar M.N., Impact of Hall Current, Dufour and Soret on transient MHD flow past an inclined porous plate: Finite element method, Materials Today: Proceedings, Volume 59, Part 1, 2022, Pages 1009-1021, ISSN 2214-7853, https://doi.org/10.1016/j.matpr.2022.02.279.
[32] Liaqat Ali, Bagh Ali, Danial Habib, Qasem Al Mdallal, Finite element analysis on the thermo-convective non-isothermal nanofluid flow in MHD Hall generator system with Soret and Dufour effects, Case Studies in Thermal Engineering, Volume 39, 2022, 102389, ISSN 2214-157X, https://doi.org/10.1016/j.csite.2022.102389.
[33] Satya Narayana, B. Venkateswarlu, S. Venkataramana, Effects of Hall current and radiation absorption on MHD micropolar fluid in a rotating system, Ain Shams Engineering Journal, Volume 4, Issue 4, 2013, Pages 843-854, ISSN 2090-4479, https://doi.org/10.1016/j.asej.2013.02.002.
[34] Seth GS, Mahato GK, Sarkar S. Effects of Hall current and rotation on MHD natural convection flow past an impulsively moving vertical plate with ramped temperature in the presence of thermal diffusion with heat absorption. Int. J. Energy Tech. 2013;5(16):1–12.
[35] Seth, S. Sarkar, S.M. Hussain, Effects of Hall current, radiation and rotation on natural convection heat and mass transfer flow past a moving vertical plate, Ain Shams Engineering Journal, Volume 5, Issue 2, 2014, Pages 489-503, ISSN 2090-4479, https://doi.org/10.1016/j.asej.2013.09.014.
[36] Bargal, M.H.S., Ben-Bansour, R., Maher, H. et al. Thermohydraulic investigation of graphene quantum dots nanofluids in a novel microchannel heat sink with a combination of elliptical ribs, secondary channels, and sinusoidal cavity. J Therm Anal Calorim (2025). https://doi.org/10.1007/s10973-025-14166-z
[37] Khalid, S.U., Nasir, M.A., Aqeel, M. et al. Thermal and hydraulic performance evaluation of heat sinks using nanofluids and innovative vortex generating fins. J Therm Anal Calorim 150, 4405–4427 (2025). https://doi.org/10.1007/s10973-024-13881-3.

[38] Deka B, Choudhury R. MHD stream past an inclined surface with diffusion-thermo and viscous dissipation sequels. J Ther Eng 2025;11(3):800–810.
[39] Hari R. Kataria, Harshad R. Patel, Radiation and chemical reaction effects on MHD Casson fluid flow past an oscillating vertical plate embedded in porous medium, Alexandria Engineering Journal, Volume 55, Issue 1, 2016, Pages 583-595, ISSN 1110-0168, https://doi.org/10.1016/j.aej.2016.01.019.
[40] Hari R. Kataria, Harshad R Patel, Soret and heat generation effects on MHD Casson fluid flow past an oscillating vertical plate embedded through porous medium, Alexandria Engineering Journal, Volume 55, Issue 3, 2016, Pages 2125-2137, ISSN 1110-0168, https://doi.org/10.1016/j.aej.2016.06.024.